Topological and MAI Constraints on the Performance of Wireless CDMA Sensor Networks

Swades De, Chunming Qiao, Dimitris A. Pados, and Mainak Chatterjee

***Abstract*— In this paper, we characterize analytically the multiaccess interference (MAI) in wireless CDMA sensor networks with uniformly random distributed nodes and study the trade-off between interference and connectivity. To provide a guideline for improving system behavior, three competitive deterministic topologies are evaluated along with the random topology in terms of link-level and network-level (routing) performance. The impact of the signature code length and the receiver design on network performance for different topologies is also studied.**

Keywords – Wireless sensor networks, ad hoc networks, code-division-multiple-access (CDMA), network connectivity, network topology, interference suppression, spreading signatures, throughput

I. Introduction and Motivation

We consider a wireless sensor network which may contain thousands of tiny low-cost sensors scattered over a region of interest [1],[2]. The sensors (also called nodes) are battery operated (i.e., energy constrained), have limited memory and processing power, and form a randomly connected *ad hoc* network. Since the nodes are mostly stationary, their location information may be obtained via GPS or other means [3]-[6] to assist efficient information processing (e.g., data aggregation) and distributed routing.

Since the sensors have limited energy, buffer space and other resources, contention-based protocols based, for example, on the 802.11 direct-sequence spread-spectrum (DS-SS) technique may not be a suitable option. Here, as an alternative, we suggest the use of several codes (signatures) that can be allocated to different nodes with possible code reuse between spatially separated nodes as in cellular CDMA systems. The use of multiple properly designed codes will reduce the channel access conflict but at the expense of multiaccess interference (MAI) which is absent in 802.11 DS-SS systems.

It is well-known that MAI is a key factor in determining the performance (e.g., throughput) of a CDMA network [7],[8]. Even if each node transmits at the lowest possible power to its intended receiver, random distribution of active (i.e., transmitting/receiving) nodes, lack of coordination (e.g., reservation [9] or request/acknowledgment [10] based transmission), and decentralized control will result in a significant amount of interference power from neighboring nodes. The interference problem becomes more severe as the node density increases, although a higher node density might otherwise help improve connectivity and network performance.

Liu and Asada [11] addressed the MAI issue in DS-CDMA based sensor networks by attempting to minimize MAI through minimum energy channel coding and on-off keying data transmission. In this approach, to deal with higher number of users, MAI is controlled by increasing the number of redundant bits (that is, lowering the channel code rate) at the cost of reduced information transmission rate. In [12], Dousse *et al.* assumed a TDMA-based channel access scheme on top of the CDMA codes to address the interference-related connectivity problem in a large ad hoc network. Muqattash and Krunz [13] proposed a controlled access CDMA protocol for wireless ad hoc networks where out-of-band RTS-CTS (request-to-send/clear-to-send) packets are used to determine MAI before a data packet transmission and then adjust the transmission power accordingly. In terms of network connectivity, Bettstetter [14] studied the relationship between k-connectivity and node density for a uniformly random node distribution, where a graph is said to be k-connected ($k \geq 1$) if for each node pair there exist at least k mutually independent paths connecting them. Yet, along with these studies, one also needs to consider the physical and medium-access-control (MAC) layer constraints so that for a given receiver structure and for an acceptable packet error performance, an optimum network topology can be determined (or for a given network topology an optimum receiver can be designed to achieve a target error performance).

In this work, we first characterize theoretically the MAI in a network with a random topology and study the associated trade-off with k-connectivity. Instead of controlling MAI at the channel code design level, we propose to control MAI to a certain extent by proper placement/activation of nodes for a given signature code set and receiver structure, while maintaining the desired graph connectivity. To this end, we study the link-level (i.e., single-hop) bit error rate (BER) performance of different network topologies, such as random, hexagonal, square grid, and triangular, using conventional matched-filter (MF) as well as MAI suppressive minimum-mean-square-error (MMSE) receivers [16] under Gold [17] or other recently identified minimum total-squared-

Swades De is with the Dept. of Electrical Eng., State University of New York at Buffalo; email: swadesd@eng.buffalo.edu. Chunming Qiao is with the Dept. of Computer Sc. and Eng., State University of New York at Buffalo; email: qiao@cse.buffalo.edu. Dimitris A. Pados is with the Dept. of Electrical Eng., State University of New York at Buffalo; email: pados@eng.buffalo.edu. Mainak Chatterjee is with the Dept. of Electrical and Computer Eng., University of Central Florida; email: mainak@cs.ucf.edu.

correlation (minTSC) code assignments [18]. Then, we study the network level performance (end-to-end throughput) of the various topologies under the two different receiver designs and signature code assignments.

Based on our evaluation, we draw the following conclusions: (a) To ensure the least requirement of 1-connectivity, the random topology needs a significantly larger number of nodes compared to the regular topologies. (b) To simplify the receiver structure and reduce the signature code length, strategic node placement/activation is important. On the other hand, with randomly placed/activated nodes, MAI suppressive receivers using a longer code length (associated with higher cost and longer processing delay) are necessary. (c) Although the triangular topology requires slightly higher number of nodes and has slightly lower MAI performance compared to the other two regular topologies, it has superior overall end-to-end routing performance with graceful degradation in the presence of node failures. (d) Maintaining a regular topology is important in that beyond a certain node failure rate the routing performance of a regular topology can be significantly inferior to that of a random topology (which is more dense). We note that it may be difficult to achieve and maintain a regular topology in certain field scenaria. Yet, it is still important to study the performance of regular topologies since they give bounds on the performance that practical sensor networks can achieve and offer guidelines to desirable node placement/activation strategies.

The rest of this paper is organized as follows. In Section II, we derive the interference power distribution at a receiver in a CDMA-based sensor network where the nodes are uniformly randomly distributed. In Section III, the k-connectivity versus MAI trade-off in a random topology network is discussed and the three competitive regular topologies (hexagonal, square grid, and triangular) are introduced. The impact of the physical-layer receiver and signature code length on the link-level and routing performance of various network topologies is studied in Section IV. Other related work is described in Section V and a few concluding remarks are given in Section VI.

II. MAI Analysis for Randomly Distributed Nodes

We assume that each node is assigned a unique binary signature code. Because of non-zero cross-correlation between different signatures, there must be an upper limit on the number of simultaneously active nodes in the vicinity of a receiver (i.e., within the interference range of a receiver) so that the received signal-to-interference-and-noise-ratio (SINR) is above a minimum operational threshold. Because of the assumed random distribution of nodes it is not possible to obtain a deterministic number of simultaneously active nodes for a given SINR. Therefore, we obtain the statistical distribution of interference power from a neighbor at the receiver under consideration, from which the expected interference at a receiver can be obtained for a given node density. Note that we do not consider signature codes with perfectly zero cross-correlation (such as the Walsh-Hadamard code sets) because of (*i*) the restriction in the number of available Walsh-Hadamard codes (less than or equal to the given multiple-of-four code length) and (*ii*) the loss of orthogonality in practice due to physical layer asynchronicity and/or multipath signal propagation.

To obtain the interference power distribution, we use the following assumptions and definitions.

- All nodes have an omni-directional transmit and receive antenna of the same gain.
- The *receiving distance* r_R is defined as the maximum distance from which a receiving node can correctly recover a transmitted signal.
- The *interference distance* r_I is defined as the maximum distance from which a receiving node can be interfered. Typically, $r_I \approx 2r_R$ [19].
- With high probability, only one of the nodes within a certain minimum distance $r_0 \geq 1$ *unit* is active (i.e., participates in sensing and routing activities). When $r_0 << r_R$, we can safely assume that the spatial distribution of active nodes remains uniformly random.
- The signal power level at each receiver is controlled by the corresponding transmitter and is equal to the lowest operational threshold. Since the internodal distance varies randomly, the required transmit power is different for different transmitter-receiver pairs.

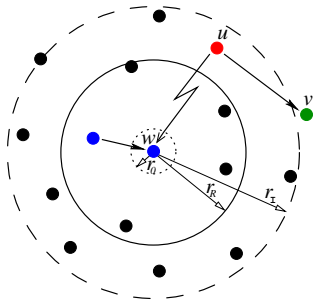

Fig. 1. MAI at node w from local neighbor u.

Fig. 1 shows node w as the receiver under consideration. Node u, while transmitting to node v, acts as an interferer to node w.

In the following, unless otherwise stated, a variable in bold denotes a random variable (RV) and a variable in italics denotes a sample value.

A. Distribution of Interference Power

Let the maximum range of a node be denoted by r. For correct signal recovery, $r = r_R$; in terms of collecting interference, $r = r_I$. If r_0 is the minimum distance between two active nodes, the cumulative distribution function (cdf) of the inter-nodal distance $\mathbf{x}$ under uniform random placement

in a two-dimensional space is given by

$$F_{\mathbf{x}}(x) = \begin{cases} \frac{x^2-r_0^2}{r^2-r_0^2}, & \text{in } (r_0,\ r] \\ 1, & x > r \\ 0, & x \le r_0. \end{cases}$$

The corresponding probability density function (pdf) is

$$f_{\mathbf{x}}(x) = \begin{cases} \frac{2x}{r^2-r_0^2}, & \text{in } (r_0,\ r] \\ 0, & \text{elsewhere.} \end{cases}$$

With the knowledge that signal power in wireless media decays proportionally to the distance raised to the n-th power where n varies between two and six, let us define the RV $\mathbf{y} \triangleq \mathbf{x}^n$. The cdf of $\mathbf{y}$ is

$$F_{\mathbf{y}}(y) = \begin{cases} F_{\mathbf{x}}(y^{\frac{1}{n}}), & \text{in } (r_0^n,\ r^n] \\ 1, & y > r^n \\ 0, & y \le r_0^n. \end{cases}$$

From the above,

$$f_{\mathbf{y}}(y) = \begin{cases} \frac{2y^{\frac{2}{n}-1}}{n(r^2-r_0^2)}, & \text{in } (r_0^n,\ r^n] \\ 0, & \text{elsewhere.} \end{cases} \quad (1)$$

To determine the distribution of the transmit power from a node u to a local neighbor v, $\mathbf{p_{t,uv}}$, we note that to achieve a desired receive power threshold P_r, the required transmit power $\mathbf{p_{t,uv}}$ increases with the n-th power of the distance d_{uv}. Ignoring shadowing effects (which will be considered later in Section IV), the receive power $\mathbf{p_{t,uv}}$ is related to P_r as follows:

$$\mathbf{p_{t,uv}} = P_r \mathbf{d}_{\mathbf{uv}}^n, \quad r_0 < d_{uv} \le r_R. \quad (2)$$

P_r being constant, $\mathbf{p_{t,uv}}$ is a RV in $(P_r r_0^n,\ P_r r_R^n]$ with pdf

$$f_{\mathbf{p_{t,uv}}}(p_t) = \begin{cases} \frac{2p_t^{\frac{2}{n}-1}}{nP_r^{\frac{2}{n}}(r_R^2-r_0^2)}, & P_r r_0^n < p_t \le P_r r_R^n \\ 0, & \text{elsewhere.} \end{cases} \quad (3)$$

Referring to Fig. 1, the distance of the interfering transmitter u from node w, $\mathbf{d_{uw}}$, is a RV in $(r_0,\ r_I]$ and the interfering receive power at node w due to transmitter u is given by

$$\mathbf{p_I} = \frac{P_r \mathbf{d}_{\mathbf{uv}}^n}{\mathbf{d}_{\mathbf{uw}}^n}, \quad r_0 < d_{uv} \le r_R,\ r_0 < d_{uw} \le r_I. \quad (4)$$

In Fig. 2, the horizontal axis represents the RV $\mathbf{p_{t,uv}}$ and the vertical axis represents the RV $\mathbf{d_{uw}^n}$. Three different regions (zones) can be identified as follows. Zone 1 corresponds to the case $\frac{P_r r_0^n}{r_I^n} < p_I < \frac{P_r r_R^n}{r_I^n}$, Zone 2 to the case $\frac{P_r r_R^n}{r_I^n} \le p_I < P_r$, and Zone 3 to the case $P_r \le p_I < \frac{P_r r_R^n}{r_0^n}$. With this breakdown, the cdf of $\mathbf{p_I}$ is obtained as follows.

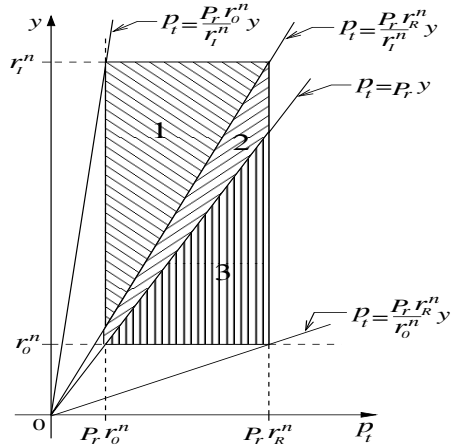

Fig. 2. Pictorial representation of the relation between $\mathbf{p_{t,uv}}$ and $\mathbf{d_{uw}^n} \triangleq \mathbf{y}$ where $p_t \sim (P_r r_m^n,\ P_r r_R^n]$, $y \sim (r_0^n,\ r_I^n]$.

Zone 1: $\frac{P_r r_0^n}{r_I^n} < p_I < \frac{P_r r_R^n}{r_I^n}$.

$$\begin{aligned} &F_{\mathbf{p_I}}\left(p_I \,\middle|\, \tfrac{P_r r_0^n}{r_I^n} < p_I < \tfrac{P_r r_R^n}{r_I^n}\right) \\ &= \int_{y=\frac{P_r r_0^n}{p_I}}^{r_I^n} \int_{p_t=P_r r_0^n}^{y p_I} f_{\mathbf{p_{t,uv}}}(p_t)\, f_{\mathbf{y}}(y) dp_t dy \\ &= \frac{r_I^4 p_I^{\frac{2}{n}} + P_r^{\frac{4}{n}} r_0^4 p_I^{-\frac{2}{n}} - 2P_r^{\frac{2}{n}} r_0^2 r_I^2}{2P_r^{\frac{2}{n}}(r_I^2-r_0^2)(r_R^2-r_0^2)}. \end{aligned} \quad (5)$$

Zone 2: $\frac{P_r r_R^n}{r_I^n} \le p_I < P_r$.

$$\begin{aligned} &F_{\mathbf{p_I}}\left(p_I \,\middle|\, \tfrac{P_r r_R^n}{r_I^n} \le p_I < P_r\right) \\ &= \int_{y=\frac{r_0^n r_I^n}{r_R^n}}^{r_I^n} \int_{p_t=P_r r_0^n}^{\frac{P_r r_R^n}{r_I^n} y} f_{\mathbf{p_{t,uv}}}(p_t)\, f_{\mathbf{y}}(y) dp_t dy \\ &\quad + \int_{p_t=P_r r_0^n}^{P_r r_R^n} \int_{y=\frac{p_t}{p_I}}^{\frac{r_I^n p_t}{P_r r_R^n}} f_{\mathbf{p_{t,uv}}}(p_t)\, f_{\mathbf{y}}(y) dy dp_t \\ &= \frac{r_I^2}{(r_I^2-r_0^2)} - \frac{(r_R^2+r_0^2)}{2(r_I^2-r_0^2)} P_r^{\frac{2}{n}} p_I^{-\frac{2}{n}}. \end{aligned} \quad (6)$$

Zone 3: $P_r \le p_I < \frac{P_r r_R^n}{r_0^n}$.

$$\begin{aligned} &F_{\mathbf{p_I}}\left(p_I \,\middle|\, P_r \le p_I < \tfrac{P_r r_R^n}{r_0^n}\right) \\ &= 1 - \int_{p_t=r_0^n p_I}^{P_r r_R^n} \int_{y=r_0^n}^{\frac{p_t}{p_I}} f_{\mathbf{p_{t,uv}}}(p_t)\, f_{\mathbf{y}}(y) dy dp_t \\ &= 1 - \frac{r_0^4 p_I^{\frac{2}{n}} + P_r^{\frac{4}{n}} r_R^4 p_I^{-\frac{2}{n}} - 2P_r^{\frac{2}{n}} r_0^2 r_R^2}{2P_r^{\frac{2}{n}}(r_I^2-r_0^2)(r_R^2-r_0^2)}. \end{aligned} \quad (7)$$

Hence, from (5), (6), and (7), the pdf of $\mathbf{p}_I$ is

$$f_{\mathbf{p_I}}(p_I) = \begin{cases} \frac{r_I^4 p_I^{\frac{2}{n}-1} - P_r^{\frac{4}{n}} r_0^4 p_I^{-\frac{2}{n}-1}}{nP_r^{\frac{2}{n}}(r_I^2-r_0^2)(r_R^2-r_0^2)}, & \frac{P_r r_0^n}{r_I^n} < p_I < \frac{P_r r_R^n}{r_I^n} \\ \frac{P_r^{\frac{2}{n}}(r_R^2+r_0^2)}{n(r_I^2-r_0^2)} p_I^{-\frac{2}{n}-1}, & \frac{P_r r_R^n}{r_I^n} \le p_I < P_r \\ \frac{P_r^{\frac{4}{n}} r_R^4 p_I^{-\frac{2}{n}-1} - r_0^4 p_I^{\frac{2}{n}-1}}{nP_r^{\frac{2}{n}}(r_I^2-r_0^2)(r_R^2-r_0^2)}, & P_r \le p_I < \frac{P_r r_R^n}{r_0^n}. \end{cases} \quad (8)$$

An illustrative example to be followed throughout the rest of our presentation is given below.

Example : Consider $r_R = 25\ m$, $r_I = 56\ m$, $r_0 = 1\ m$, $n = 3.0$, and $P_r = -70$ *dBm* (more on the choice of r_I in relation to r_R and n will be discussed in Section IV). The pdf of $\mathbf{p}_I$ as given in (8) is shown in Fig. 3. The Monte-Carlo simulated pdf plot is obtained by randomly placing 2700 nodes in a 627.87×537.5 m^2 rectangular area. Simulation and analytic results match well. In the very low interference power region there is a lack of sufficient simulation data because the probability of having a given transmitter-receiver pair decreases with distance. □

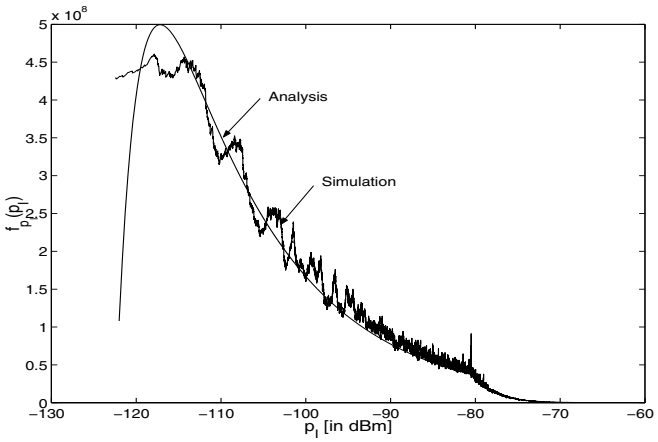

Fig. 3. Analytical (eq. (8)) and simulated distribution of $\mathbf{p}_I$ ($r_0 = 1\ m$, $r_R = 25\ m$, $r_I = 56\ m$, $n = 3.0$, and $P_r = -70$ *dBm*).

Using our findings in (8), the mean value of the collected interference power η from an interfering node is given by

$$\eta = \frac{4P_r\left(r_R^{n+2} - r_0^{n+2}\right)\left(r_I^{n-2} - r_0^{n-2}\right)}{(n^2-4)r_0^{n-2}r_I^{n-2}\left(r_I^2 - r_0^2\right)\left(r_R^2 - r_0^2\right)} \tag{9}$$

for $2 < n \leq 6$. Note that since in practice $n > 2$, we do not consider the case $n = 2$ which can be easily dealt with as a special case.

Example (continued) : From (9) we obtain $\eta = -64.06$ *dBm*. Fig. 4 shows the impact of r_0 on the average interference power collected from a neighbor when r_0 varies from $1\ m$ to $7\ m$. We observe that decrease of r_0 increases the average interference power at a higher than linear rate.

We now proceed to obtain an expression for the average number of potential interfering neighbors around a receiver.

B. Number of Potential Interfering Neighbors

The area covered by the interference range of a receiver (for example, node w in Fig. 1) is $a_I = \pi r_I^2$. If there are N nodes that are uniformly randomly distributed over a region of area A, the probability that a node has n neighbors within the interference range is binomially distributed:

$$\Pr[n \text{ neighbors}] = \binom{N-1}{n}\left(\frac{a_I}{A}\right)^n\left(1 - \frac{a_I}{A}\right)^{N-n-1}. \tag{10}$$

For $N >> 1$ and $a_I << A$, the above binomial distribution is well approximated by the Poisson distribution. Thus,

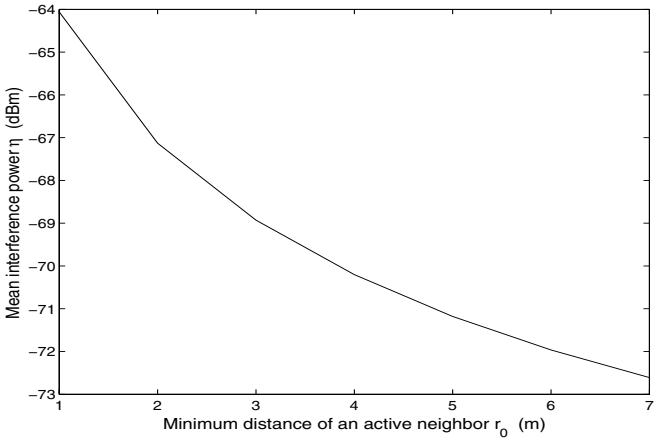

Fig. 4. Mean interference power from a neighboring transmitter (eq.(9)). As in Fig. 3, $r_R = 25\ m$, $r_I = 56\ m$, $n = 3.0$, and $P_r = -70$ *dBm*.

$$\Pr[n \text{ neighbors}] \approx \frac{(\rho a_I)^n}{n!}e^{-\rho a_I} \tag{11}$$

where $\rho = \frac{N}{A}$ is the node density. Under the Poisson approximation, the expected number of nodes within the interference range of the receiver is

$$\begin{aligned} K &= \sum_{n=0}^{N-1} n\frac{(\rho a_I)^n}{n!}e^{-\rho a_I} \\ &= \rho\pi r_I^2 \quad \text{for } N >> 1 \text{ and } a_I << A. \end{aligned} \tag{12}$$

Example (continued) : With $N = 2700$, $A = 627.87 \times 537.5\ m^2$, and $r_I = 56\ m$ as before, we obtain a mean number of nodes within the interference range of a receiver $K = 79$. Note that only a fraction of the mean number of K nodes will be actual interferers and this fraction depends on node transmission activity and failure probability. We do not attempt to calculate analytically the average number of actual interferers at this time. The actual interferers will be determined as necessary in simulation-based performance studies in Section IV. □

With the above observations, we are now ready to examine the network k-connectivity issue.

III. k-CONNECTIVITY

Following Bettstetter [14], we note that degree of connectivity k implies that for all nodes in the network the minimum number of neighbors k_{min} is greater than or equal to k. For uniformly randomly distributed nodes we can calculate

$$\begin{aligned} \Pr[k_{min} \geq k] &\equiv \Pr[\text{all nodes have at least } k \text{ neighbors}] \\ &= \left(1 - \sum_{n=0}^{k-1}\frac{(\rho a_R)^n}{n!}e^{-\rho a_R}\right)^N \end{aligned} \tag{13}$$

where $a_R = \pi r_R^2$.

However, it is well understood that all nodes having $k_{min} \geq k$ does not ensure that the graph (network) is k-connected. There can be isolated islands of nodes (forming a multi-component graph) with each node still satisfying $k_{min} \geq k$. Thus,

$$\Pr[k\text{-connectivity}] \leq \Pr[k_{min} \geq k].$$

For asymptotically large networks ($N \to \infty$), Penrose [20] proved that

$$k\text{-connectivity} \quad \underset{\text{in prob.}}{\overset{N \to \infty}{\longrightarrow}} \quad k_{min} \geq k, \tag{14}$$

i.e., $\Pr[k_{min} \geq k]$ is a tight upperbound of the probability of k-connectivity of a network.

A. MAI versus k-Connectivity

As we have stated in the introduction, we are interested in studying the trade-off between connectivity (for successful routing) and MAI. We continue with the example introduced in the previous section and demonstrate the effect of MAI reduction on network connectivity for randomly distributed nodes.

Example (continued) : We recall that $N = 2700$ and $A = 627.87 \times 537.5\ m^2$, which gives $\rho = 0.008$. With $r_0 = 1\ m$, (11) with a_I set equal to $a_0 = \pi r_0^2$ gives Pr[no nodes within r_0 range] = 0.9752. With $r_R = 25\ m$, (13) gives Pr[$k_{min} \geq 1$] = 0.9996. Therefore, under this setting, the network satisfies 1-connectivity (with probability 99.9%) and at the same time (with probability 97.5%) there is no active node within $1\ m$ of the receiver. To further reduce the interference power (cf. Fig. 4), let $r_0 = 2\ m$ and keep Pr[no nodes within r_0 range] = 0.9752; the required node density ρ becomes 0.002 or N becomes 675 for the given fixed deployment area A. If the receiving range r_R of a node is kept fixed at $r_R = 25\ m$, we have $\Pr[k_{min} \geq 1] = 1.47 \times 10^{-6}$. Hence, the nodes are virtually isolated. □

The above example shows that if the active nodes remain randomly uniformly distributed, then it is not possible to maintain a desired high degree of network connectivity and have low MAI at the same time. In this context, we suggest that for a given (high) node density at the time of deployment, low MAI and high connectivity can be achieved when the nodes are selectively activated such that *the set of active nodes at any time lie on the vertices of a regular polygon*. The regular polygon can be a square grid, a hexagon, or an equilateral triangle, for example. From Fig. 5, it is clear that with no node failures, the hexagonal topology offers 3-connectivity, the grid topology offers 4-connectivity, and the triangular topology offers 6-connectivity. We note that although we may not be able to achieve and maintain a regular topology in certain field applications, the performance of regular topologies (with no node failures) offer important bounds on the performance of practical sensor networks with distributed control.

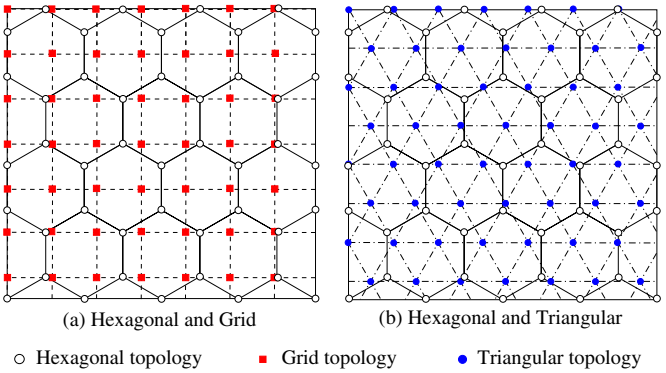

Fig. 5. Various regular network topologies. The internodal distance in all topologies remains the same (r_R).

In the following section, we study the relative MAI and routing performance of the three regular topologies (hexagonal, grid, and triangular) and compare with the random topology.

IV. Performance Studies

To study the relative performance of random and regular topologies, we assume that the receiving range of a node r_R is equal to the arm length of a regular polygon (hexagon, grid, and triangle). The interference range is considered to be $r_I = \sqrt{5} r_R$. Within the $r_I = \sqrt{5} r_R$ range, the hexagonal topology has 12 nodes, the grid topology has 20 nodes, the triangular topology has 18 nodes, and the random topology has 79 nodes on average (see (12) and the related example).

To determine the number of nodes required in different regular topologies to cover an area A, we start with the hexagonal topology where $N_{hex} = 2(M+1)^2$ nodes are placed over an $A = \left\lceil \frac{(2M+1)\sqrt{3} r_R}{2} \right\rceil \times \left\lceil \frac{(3M+1) r_R}{2} \right\rceil$ rectangular area for some integer M. In Fig. 5(a), for example, $M = 4$ and $N_{hex} = 50$. The number of active nodes required for the grid topology is $N_{sqr} = \lfloor \frac{\sqrt{3}(2M+1)}{2} + 1 \rfloor \lfloor \frac{3M+1}{2} + 1 \rfloor$. The corresponding number for the triangular topology is $N_{tri} = \lfloor \frac{\sqrt{3}(2M+1)}{2} + 1 \rfloor \lfloor \frac{3M+1}{2\sqrt{3}} + 1 \rfloor + \lfloor \frac{\sqrt{3}(2M+1)-1}{2} + 1 \rfloor \lfloor \frac{(3M+1)-\sqrt{3}}{2\sqrt{3}} + 1 \rfloor$. The number of nodes, N_{rnd}, required for the random topology to fill in the same rectangular space while ensuring 1-connectivity with high probability can be obtained from (13) where $\rho = \frac{N_{rnd}}{A}$. Table I shows that the regular topologies achieve a significant gain with respect to the random topology in terms of number of nodes required to cover a given deployment area with a network of connectivity at least one.

TABLE I
NUMBER OF NODES REQUIRED IN DIFFERENT TOPOLOGIES
($A = 627.87 \times 537.5\ m^2$; $r_R = 25\ m$)

Hexagonal (3-connected)	Square grid (4-connected)	Triangular (6-connected)	Random (1-connected with probability 0.9996)
450	572	638	2700

In the sequel, we study the system performance of the four network topologies in Table I with respect to the following system parameters: (a) signature codes, (b) receiver type, and (c) CDMA signal synchronism.

Signature Codes: We consider *Gold sequences* [17] of chip length $L = 63$ which can support up to 65 users. In pursue of low computational cost receiver operations, we also consider *minimum total-squared-correlation (minTSC) codes* [18] of chip length $L = 15$ that are available for any number of signatures/users up to $2^{L-1} = 2^{14}$. When using a minTSC code set of length 15 in a regular topology, the receiver signal set-up remains mostly underloaded (i.e., the number of interfering neighbors K_I does not exceed 15). In contrast, in a random topology, the receivers are mostly overloaded (i.e., $15 < K_I$).

CDMA Receiver: First, we consider the conventional matched-filter (MF) which is simple to realize but may be rather ineffective in the presence of moderate to severe MAI. Then, we consider active MAI suppression via minimum-mean-square-error (MMSE) filtering [16] which can be particularly important under overloaded signal conditions.

Signal Synchronization: Physical layer node/user CDMA signals can be either bit-synchronous or bit-asynchronous We study the both cases over the underlying assumption of chip-synchronicity.

In addition, we study the system performance in presence (or absence) of log-normal shadowing. The log-normal path loss is calculated considering isotropic antennas of unity gain and operating frequency $f = 4$ *GHz*. Assuming that (for tiny sensors) the largest physical linear dimension of the antenna is $D \approx 1$ *cm*, we obtain the Fraunhofer distance value [21, Chapter 3] $d_f = \frac{2D^2}{\lambda} << 1\ m$ which verifies that the nodes outside $r_0 = 1\ m$ are indeed in the far field region where the log-normal path loss equation is valid ($\lambda = \frac{c}{f}$ is the operating wavelength where c is the speed of light in free space). The path loss up to $r_0 = 1\ m$ is obtained via the Friis free space equation [21, Chapter 3]. The standard deviation of the channel disturbance due to log-normal shadowing is considered to be $\sigma_{LN} = 8$ *dB*. A fading margin of 8 *dB* is set when log-normal shadowing is taken into account.

We use binary-phase-shift-keying (BPSK) CDMA modulation. The desired receive power threshold is $P_r = -70$ *dBm* and the white Gaussian thermal noise power at the receiver is $\sigma^2_{Th} = -80$ *dBm*. Hence, the desired SNR (signal-to-noise ratio) threshold is 10 *dB*. Unless otherwise stated, the transmission probability of a node is fixed at $Tx = 0.5$. Below, we study the link-level (i.e., one-hop) BER performance in the presence of MAI via simulations.

A. Link-level Error Performance

When studying the link level BER performance, we pick the receiver under consideration to be located well within the boundaries of the 627.87×537.5 m^2 field (i.e., at least $(r_I + r_R)\ m$ away from any boundary) to ensure that none of the potential interferers faces the border effect [14].

For the random topology, only one of the nodes within $r_0 = 1\ m$ of one another is considered potentially active. For the regular topologies, there are certain deterministic interference signal power levels depending on the location of the interfering transmitters. For example, in the hexagonal topology there are at most *two* interferers with SNR= 10 *dB* (at distance r_R), at most *six* interferers with SNR= 2.84 *dB* (at distance $\sqrt{3}r_R$), and at most *three* interferers with SNR= 0.97 *dB* (at distance $2r_R$).

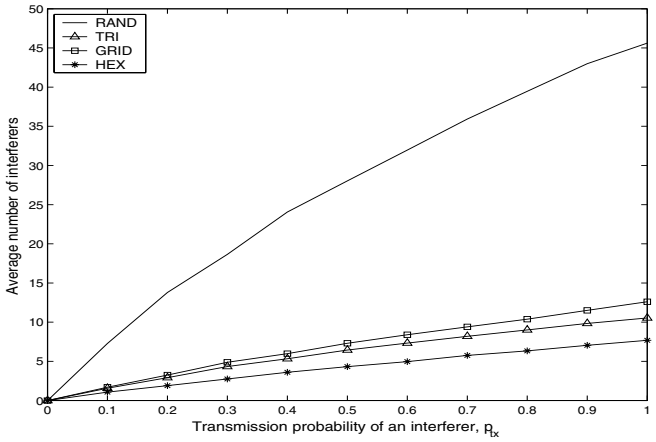

Fig. 6. Average number of interferers versus node transmission probability (idling/failure/sleeping node probability $P_f = 0$).

Fig. 6 shows the average number of interferers as a function of the transmission probability Tx for the four different topologies. When $Tx = 1$, the maximum and minimum observed number of interferers in the random topology are 62 and 35, respectively. For the grid topology, these numbers are 16 and 12 and are maximum among the regular topologies when $r_I = \sqrt{5}r_R$. Therefore, when using the low-cost short minTSC code set, the receivers of a regular topology remain mostly underloaded whereas in the random topology they are heavily overloaded.

Fig. 7 shows the relative performance of the three regular topologies, hexagonal, grid, and triangular, with MF receivers and L=63 Gold codes. With asynchronous signals, the hexagonal topology performs the best irrespective of shadowing effects as its number of potential interferers is much less ($K = 12$) compared to the triangular ($K = 18$) and grid ($K = 20$) topologies, respectively. We also note that even though the triangular topology has slightly fewer potential interferers, its MAI performance is somewhat inferior to the grid topology. This is because in the triangular topology, the interference SNR values at the receiver from farther away interferers are higher than the values for the grid (due to node placement, cf. Fig. 5). For synchronous systems, performance differences are minimal and not worth mentioning. Also, we do not present the BER plots for MMSE receivers since under all circumstances all three topologies have nearly indistinguishable performance.

With the understanding that among the three regular

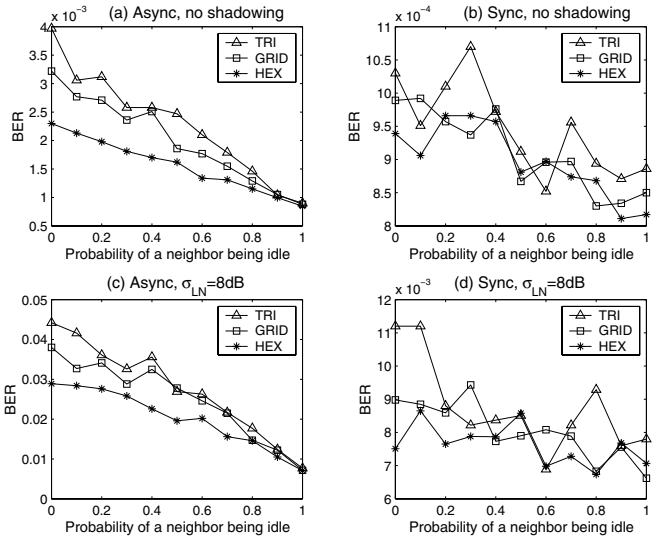

Fig. 7. Link-level BER performance of regular topologies with MF receiver and Gold codes (L=63).

topologies the link-level BER performance of the triangular topology is the worst, we will compare the performance of the random topology to the triangular. In Fig. 8, we

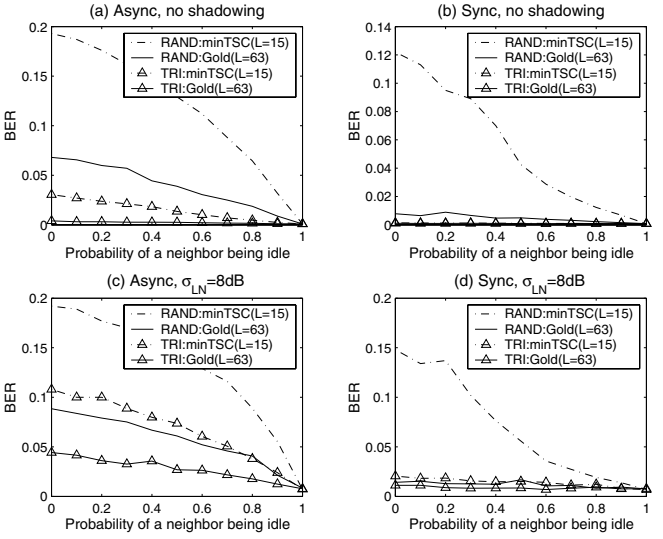

Fig. 8. Comparison of link-level BER performance of the random and triangular topology when using MF receivers.

observe that in both asynchronous and synchronous MF receiver systems the random topology performs worse than the triangular with either short ($L = 15$) minTSC or long ($L = 63$) Gold codes. In the absence of shadowing effects and in both asynchronous and synchronous systems, the random topology with the long Gold codes performs worse than the triangular topology with the short minTSC codes. In the presence of shadowing, the triangular topology with minTSC codes becomes slightly worse than the random with Gold, indicating some sensitivity to channel conditions when short codes ($L = 15$) are used.

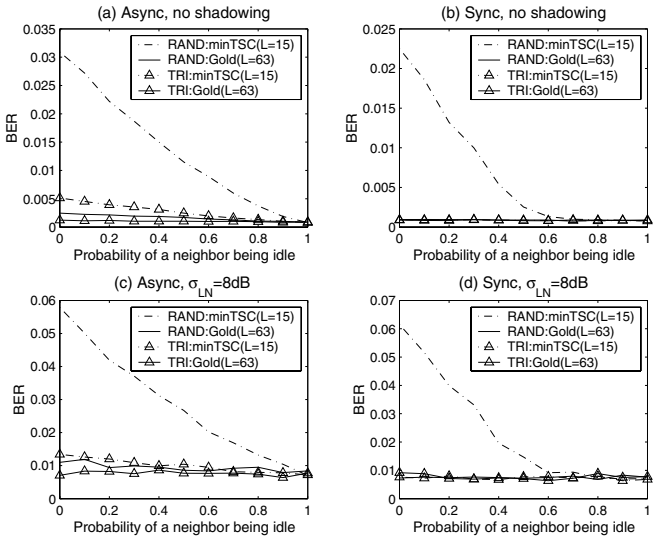

Fig. 9. Comparison of link-level BER performance of the random and triangular topology when using MMSE receivers.

When considering the interference suppressing MMSE receiver (Fig. 9), we observe that the triangular topology with short minTSC codes (L=15) performs practically the same as the random topology with long Gold codes (L=63) with or without shadowing.

With these observations, we now study the end-to-end throughput performance of a network with different topologies, codes, and receiver structures.

B. Topology-Dependent Routing Performance

To compare the routing efficiency of the three regular topologies in absence of node failures, we calculate the actual distances that are covered by an equal number of hops (i.e., equal transmit-receive energy consumption). Referring to Fig. 5, we consider routing along 12 equispaced directions that are 30° apart, starting at 0° with respect to the horizontal axis.

Along $0°$ *and* $180°$: $2H$ hops in hexagonal topology covers $\sqrt{3}Hr_R$ distance. H hops in both grid and triangular topology cover Hr_R distance. Thus, in an equal number of hops (i.e., $2H$), the ratio of distances covered in the hexagonal, grid, and triangular topology is $\sqrt{3} : 2 : 2$.

Along $30°$, $150°$, $210°$, *and* $330°$ (for the grid topology the true angles are off by 0.06%) : $4H$ hops in hexagonal topology covers $3Hr_R$ distance; $41H$ hops in grid topology covers $\sqrt{901}Hr_R$ distance; $2H$ hops in triangular topology covers $\sqrt{3}Hr_R$ distance. So, in $164H$ hops the ratio of distances covered in the three topologies is $123 : 4\sqrt{901} : 82\sqrt{3}$.

Along $60°$, $120°$, $240°$, *and* $300°$ (for the grid topology the true angles are off by 0.06%) : $2H$ hops in hexagonal topology covers $\sqrt{3}Hr_R$ distance; $41H$ hops in grid topology covers $\sqrt{901}Hr_R$ distance; H hops in triangular topology

covers Hr_R distance. Therefore, in $82H$ hops the ratio of distances covered is $41\sqrt{3} : 2\sqrt{901} : 82$.

Along 90° *and* 270° *:* $4H$ hops in hexagonal topology covers $3Hr_R$ distance; H hops in grid topology covers Hr_R distance; $2H$ hops in triangular topology covers $\sqrt{3}Hr_R$ distance. Therefore, in $4H$ hops the ratio of distances covered is $3 : 4 : 2\sqrt{3}$.

Considering all 12 cases above together, for an equal number of hops (i.e., $164H$) along any of these 12 specific directions, the ratio of actual distances covered in the hexagonal, grid, and triangular topology is $1 : 1.02 : 1.16$. We recall (Table I) that the ratio of the number of nodes required to cover a given rectangular area in the three topologies is $1 : 1.27 : 1.42$. Thus, while the grid topology requires quite a larger number of nodes to cover a given area, in the absence of node failures, the grid covers only a marginally longer distance than the hexagonal topology in equal number of hops. The triangular topology, with a relatively small number of extra nodes, covers a much larger distance.

To study the relative end-to-end routing performance via simulation, we consider the same 627.87×537.5 m^2 deployment area where 450, 572, 638, and 2700 nodes are placed in a hexagonal, grid, triangular, and random topology, respectively. The radio range of each node remains $r_R = 25$ m. For each topology, we simulate geographic forwarding at the network layer using GloMoSim [22]. The nodes are assumed to be location aware and local broadcasts ensure that all nodes are also aware of their local neighbors' locations. Packets are forwarded using MFR (maximum forward with fixed radius) without backward progression [23]. The radio transmission rate is 2Mbps. A packet is dropped if it cannot be forwarded further toward the final destination (due to lack of forwarding neighbors). Nodes have a fixed packet buffer of size 100 and packets are dropped (without warning) at an intermediate node if the buffer is full. For each of the experiments described below, 20 random CBR (constant bit rate) sessions were initiated with each CBR source sending 5000 packets of size 50 bytes to the destination. Our user-defined MAC layer acts only as an interface between the network and radio layers without performing any channel monitoring or related activities. In the radio layer, we incorporate the CDMA receiver of choice; log-distance path loss and log-normal fading are also modeled. Since network connectivity is highly dependent on the status of nodes (failed/sleeping/active), we conduct simulations to study the effect of node failure and awake time on routing performance. Due to lack of space, we present throughput results of a synchronous system only. Parallel conclusions are reached from delay results and for the asynchronous system.

To obtain failure-dependent routing performance, we set the node sleeping probability to zero and to attain network steady state we assume a fixed node failure-recovery probability of 0.5; i.e., we assume that a neighbor tries to take over the routing task with probability 0.5. Fig. 10 shows the throughput performance of a synchronous CDMA system

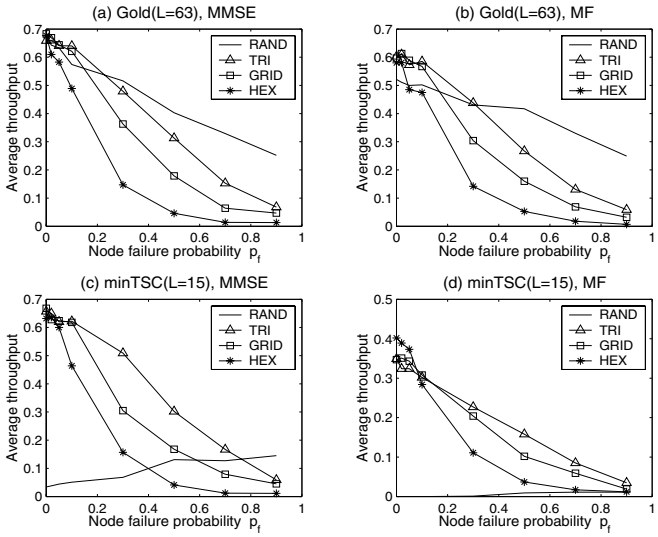

Fig. 10. Average throughput versus node failure probability in a synchronous system (failure recovery probability 0.5).

with MF or MMSE receivers and long ($L = 63$) Gold or short ($L = 15$) minTSC code sets. We observe that the performance of the regular topologies follows the same trend irrespective of receiver type and signature code set. This is because the MAI performance of the short minTSC codes in a regular topology (i.e., an underloaded system) is as good as the long Gold codes. The performance of the hexagonal topology degrades sharply with an increase in node failure probability because there are fewer nodes in this topology for route recovery. The decrease in throughput with node failure probability in the triangular topology is much slower than the other two regular topologies, indicating the highest resilience in a node failure-prone environment. We also note that in each of the regular topologies there is a "critical failure probability" up to which throughput performance is better than the random topology. This is because up to this critical failure probability point, the chance of finding a route in a regular topology is still very high whereas in the random topology MAI has not been reduced low enough. With a further increase in failure probability, routing failure in the regular topologies overrides their advantages of having low MAI, resulting in lower throughput.

Looking into the results in Fig. 10 for the random topology, we note that with the long Gold codes although the network has initially lower throughput compared to the regular topologies (due to dominant MAI effects), its performance degrades at a much slower rate. This is because there is a much larger number of nodes in the network, which can be used to find an alternate route. When using the low-cost short minTSC codes, the throughput is poor at low node failure probability because the random topology system is heavily overloaded and the short codes have little interference suppression capability. The combination short minTSC codes and MF receiver offers a sharp increase in throughput as the

node failure probability increases (not surprisingly since the pair short minTSC and MF has the least MAI resistance of all, and this cal benefit tremendously from the reduction in MAI).

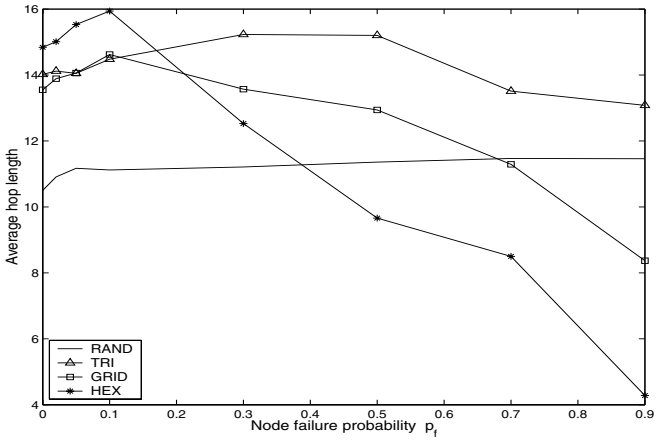

Fig. 11. Average hop length of successful routes versus node failure probability (synchronous system, Gold codes and MF receiver).

Fig. 11 shows the average hop length of successful routes as a function of the node failure probability with MF receivers and $L = 63$ Gold codes. We note that each of the regular topologies tries to recover from node failure via longer routes, yet beyond a certain failure probability only short routes can be found, which explains the results in this figure as well as in Fig. 10. Due to the substantially larger total number of nodes, the random topology is still able to recover, although the routes may be longer.

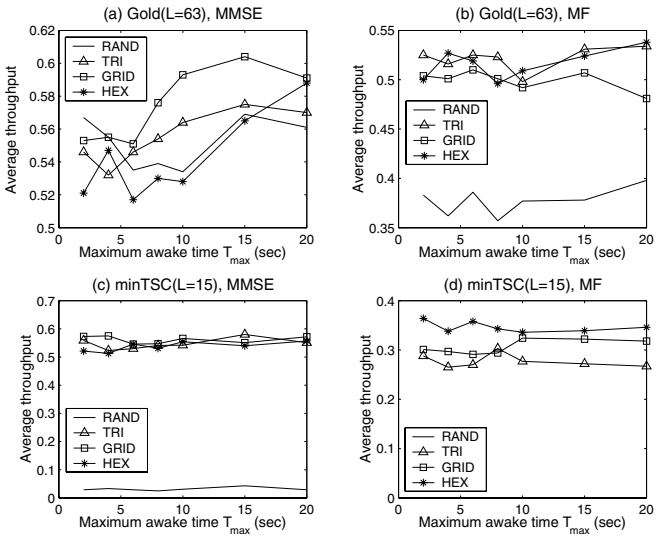

Fig. 12. Impact of sleeping behavior of a node on routing performance.

In Fig. 12, we study throughput performance as a function of the maximum node awake time T_{max}. The actual awake time is modeled by a uniform RV that takes values between 1 and T_{max} (in *sec*). Sleep time is also modeled as a uniform RV with values between 1*sec* and 2*sec*. The sleep probability is set at 0.01 and the node failure probability is zero. While the throughput of all regular topologies is relatively high and increases slightly with T_{max}, for the random topology a measurable throughput can be obtained only with the long ($L = 63$) Gold codes. This is because with the chosen parameters the MAI for the random topology is too high to be handled by the low-cost short ($L = 15$) minTSC codes.

V. Related Work

There has been a significant amount of work on cellular CDMA systems [7]. In such a scenario, to minimize the near-far effect a base station controls the transmission power of the mobile nodes under its coverage. A mobile node, however, has no control over its surrounding interfering nodes and can only ask for higher power transmission from its base station. The interference at the nodes of a sensor network is similar to that at the mobile nodes in a CDMA network. However, the sensor network problem differs in terms of the limited processing power, energy constraints, and low (or no) mobility of the sensor nodes.

Spread-spectrum techniques (DS-SS and FH-SS) have been proposed in the 802.11 standard [10] and for Bluetooth systems [24]. The primary issue addressed in these systems is interference reduction in an heterogeneous environment and not MAI management and its network layer implications.

Along these lines, Gupta and Kumar [25] analyzed the throughput capacity bounds for multihop wireless networks with a random topology. Shakkottai *et al.* [26] studied network connectivity and coverage as a function of nodal coverage and failure probability under a grid topology.

A clustering protocol for sensor networks called LEACH [27] utilizes a randomized rotation of a local cluster-head to distribute power consumption evenly among sensors. The SPAN protocol proposed by Chen *et al.* [15] provides an activity scheduling mechanism based on surrounding nodes' activity and network connectivity requirements. The SPAN approach attempts to form a hexagonal structure among the coordinator nodes and minimize the total number of nodes involved in routing (aiding to energy savings). Another energy conservation approach called Geographic Adaptive Forwarding (GAF) proposed by Xu *et al.* [28] relies on location information. The entire geographic location is divided into virtual grids and - irrespective of the density of node deployment - one node remains active within each grid to maintain network connectivity. In a two-tier data dissemination model proposed by Ye *et al.* [29], each (randomly located) data generating node divides the network into a virtual grid with itself at the corner. Each node closest to the corner of a grid acts as a potential forwarding node. In this scheme, if there is a number of geographically distributed nodes generating data, then the forwarding nodes from each grid set (due to different data generating nodes) will form a set of randomly located active nodes.

We note that although there have been individual proposals and performance studies of grid and hexagonal topologies, to the best of our knowledge, comparative studies of the regular topologies and the random topology have not been reported. Also, the triangular topology has not been considered in prior work. Our work also differs from the prior studies in the sense that we have considered the impact of receiver and code design aspects on the link-level and network-level performance.

VI. Conclusions

In this paper, we have studied the physical layer constraints on link-level and network-level performance of a wireless CDMA sensor network. We have characterized via analysis the multiaccess interference (MAI) in a random topology network and showed that high network connectivity cannot be achieved without significantly increased MAI. To achieve a good MAI versus network connectivity trade-off point, we have introduced a triangular topology. We have studied the link-level (bit error rate) as well as network-level (throughput) performance of the triangular topology as well as the hexagonal, square grid, and random topology using conventional matched-filter (MF) and MAI suppressive minimum-mean-square-error (MMSE) receivers with Gold signature code sets of length 63 and minimum total-squared-correlation (minTSC) code sets of length 15.

Our performance evaluation have showed that: (*i*) Network topology has a strong impact on potential receiver/signature design simplification (and hence, on sensor cost); (*ii*) although the triangular topology requires slightly larger number of nodes and has lower MAI performance than the other two regular topologies, its overall end-to-end routing performance is superior and has much more graceful degradation in failure-prone sensor networks; (*iii*) the benefits of a regular (for example triangular) topology are enjoyed only up to a certain node failure rate beyond which throughput performance drops sharply well below the level of a corresponding (dense) random topology.

Our results can be useful as a performance benchmark study for different node activation/deployment strategies in field sensor networks, other radio receiver designs, and minTSC signature assignments of other lengths.

Acknowledgment

The authors are thankful to Sumesh J. Philip for his help with GloMoSim simulations.

References

[1] I. F. Akyildiz, W. Su, Y. Sankarasubramaniam, and E. Cayirci, "Wireless sensor networks: A survey," *Computer Networks*, vol. 38, pp. 393–422, Mar. 2002.

[2] D. Estrin, R. Govindan, J. Heidemann, and S. Kumar, "Next century challenges: scalable coordination in sensor networks," in *Proc. ACM MOBICOM*, Seattle, WA, Aug. 1999, pp. 263–270.

[3] N. Bulusu, J. Heidemann, and D. Estrin, "GPS-less low cost outdoor localization for very small devices," *IEEE Personal Commun. Magazine*, pp. 28–34, Oct. 2000.

[4] A. Savvides, C. C. Han, and M. B. Srivastava, "Dynamic fine-grained localization in ad hoc networks of sensors," in *Proc. ACM MOBICOM*, Rome, Italy, July 2001, pp. 166–179.

[5] C. Savarese, J. Rabaey, and J. Beutel, "Locating in distributed ad hoc wireless sensor networks," in *Proc. ICASSP*, Salt Lake City, UT, May 2001, pp. 2037–2040.

[6] A. Nasipuri and K. Li, "A directionality based location discovery scheme for wireless sensor networks," in *Proc. ACM WSNA*, Atlanta, GA, Sept. 2002, pp. 105–111.

[7] A. J. Viterbi, *CDMA: Principles of Spread Spectrum Communications.* Reading, MA: Addison-Wesley, 1995.

[8] S. Gopalan, G. N. Karystinos, and D. A. Pados, "Capacity, throughput, and delay of slotted Aloha DS-CDMA links with adaptive space-time auxiliary-vector receivers," *IEEE Trans. Wireless Commun.*, to appear.

[9] D. J. Goodman, R. A. Valenzuela, K. T. Gayliard, and B. Ramamurthi, "Packet reservation multiple access for local wireless communications," *IEEE Trans. Commun.*, vol. 37, pp. 885–890, Aug. 1989.

[10] *ANSI/IEEE Standard 802.11*, Medium access control (MAC) and physical (PHY) specifications, Section 15, 1999.

[11] C.-H. Liu and H. H. Asada, "A source coding and modulation method for power saving and interference reduction in DS-CDMA sensor network systems," in *Proc. American Control Conf.*, Anchorage, AK, May 2002, pp. 3003–3008.

[12] O. Dousse, F. Baccelli, and P. Thiran, "Impact of interference on connectivity in ad hoc networks," in *Proc. IEEE INFOCOM*, San Francisco, CA, Apr. 2003, pp. 1724–1733.

[13] A. Muqattash and M. Krunz, "CDMA-based MAC protocol for wireless ad hoc networks," in *Proc. ACM MobiHoc*, Annapolis, MD, June 2003, pp. 153–164.

[14] C. Bettstetter, "On the minimum node degree and connectivity of a wireless multihop network," in *Proc. ACM MobiHoc*, Lausanne, Switzerland, June 2002, pp. 80–91.

[15] B. Chen, K. Jamieson, H. Balakrishnan, and R. Morris, "Span: An energy-efficient coordination algorithm for topology maintenance in ad hoc wireless networks," in *Proc. ACM MOBICOM*, Rome, Italy, July 2001, pp. 85–96.

[16] M. L. Honig, U. Madhow, and S. Verdu, "Blind adaptive multiuser detection," *IEEE Trans. Inform. Theory*, vol. 41, pp. 944–960, July 1995.

[17] R. Gold, "Optimal binary sequences for spread spectrum multiplexing," *IEEE Trans. Inform. Theory*, vol. 8, pp. 619–621, Oct. 1967.

[18] G. N. Karystinos and D. A. Pados, "New bounds on the total squared correlation and optimum design of DS-CDMA binary signature sets," *IEEE Trans. Commun.*, vol. 51, pp. 48–51, Jan. 2003.

[19] A. Kamerman and L. Monteban, "WaveLAN-II: A high-performance wireless LAN for the unlicensed band," *Bell Labs Tech. Journal*, vol. 2, pp. 118–133, Summer 1997.

[20] M. D. Penrose, "On k-connectivity for a Geometric Random Graph," *Wiley Random Structures and Algorithms*, vol. 15, pp. 145–164, 1999.

[21] T. Rappaport, *Wireless Communications: Principles and Practice.* Upper Saddle River, NJ: Prentice Hall, 1996.

[22] X. Zeng, R. Bagrodia, and M. Gerla, "GloMoSim: A library for parallel simulation of large-scale wireless networks," in *Proc. 12th Workshop on Parallel and Distributed Systems (PADS)*, Banff, Alberta, Canada, May 1998, pp. 154–161.

[23] S.-C. Woo and S. Singh, "Scalable routing protocol for ad hoc networks," *Wireless Networks*, vol. 7, pp. 513–529, Jan. 2001.

[24] *http://www.bluetooth.org/specifications.htm*, Nov. 2002.

[25] P. Gupta and P. R. Kumar, "The capacity of wireless networks," *IEEE Trans. Inform. Theory*, vol. 46, pp. 388–404, Mar. 2000.

[26] S. Shakkottai, R. Srikant, and N. B. Shroff, "Unreliable sensor grids: Coverage, connectivity and diameter," in *Proc. IEEE INFOCOM*, San Francisco, CA, Apr. 2003, pp. 1073–1083.

[27] W. R. Heinzelman, W. R. Chandrakasan, and H. Balakrishnan, "Energy-efficient communication protocols for wireless microsensor networks," in *Proc. Hawaiian Intl. Conf. on Systems Science*, Maui, Hawaii, Jan. 2000, pp. 3005–3014.

[28] Y. Xu, J. Heidemann, and D. Estrin, "Geography-informed energy conservation for ad hoc routing," in *Proc. ACM MOBICOM*, Rome, Italy, July 2001, pp. 70–84.

[29] F. Ye, H. Luo, J. Cheng, S. Lu, and L. Zhang, "A two-tier data dissemination model for large-scale wireless sensor networks," in *Proc. ACM MOBICOM*, Atlanta, GA, Sept. 2002, pp. 148–159.